

## Electronic conduction in ‘random’ Al–Ge films

J Shoshany<sup>†</sup>, V Goldner<sup>†</sup>, R Rosenbaum<sup>†</sup>, M Witcomb<sup>‡</sup>, D S McLachlan<sup>§</sup>,  
A Palevski<sup>||</sup>, M Karpovski<sup>||</sup>, A Gladkikh<sup>||</sup> and Y Lereah<sup>||</sup>

<sup>†</sup> School of Physics and Astronomy, Raymond and Beverly Sackler Faculty of Exact Sciences,  
Tel Aviv University, Ramat Aviv, 69978, Israel

<sup>‡</sup> University of the Witwatersrand, Electron Microscope Unit, Private Bag 3, Wits, 2050, South  
Africa

<sup>§</sup> University of the Witwatersrand, Department of Physics, Wits, 2050, South Africa

<sup>||</sup> School of Physics and Astronomy, Quantum Electronic Transport Laboratory, Raymond and  
Beverly Sackler Faculty of Exact Science, Tel Aviv University, Ramat Aviv, Tel Aviv, 69978,  
Israel

Received 28 November 1995

**Abstract.** Electronic transport properties have been measured for 3500 Å Al–Ge films with a random microstructure. The room temperature resistivity exhibits a sharp discontinuous jump at the metal–insulator transition, allowing for the direct determination of the critical metallic fraction,  $\phi_c = 8.8$  vol% Al. A new procedure is described for extracting values for the zero-temperature conductivity  $\sigma(0)$  from the low-temperature conductivity data. When  $\sigma(0)$  is extrapolated to zero as a function of Al content, the value obtained for the critical aluminium fraction  $\phi_c$  is in excellent agreement with the value obtained from the room temperature data. The films exhibit two transition regions below 1.2 K as the Al content is decreased—a transition from the superconductivity state to the normal-metallic state, followed by a second transition from the normal-metallic state to the insulating, variable-range-hopping state. Superconducting fluctuation data taken above 1.2 K were well described using the 2D Aslamazov–Larkin and Maki–Thompson formulae; the ‘resistive tails’ below 1.2 K are also discussed.

### 1. Introduction—earlier work on Al–Ge films

When Al and Ge are coevaporated upon glass substrates held at room temperature, one obtains a granular structure composed of small 20 Å to 200 Å crystalline grains of Al coated by a mantle of amorphous Ge [1]. Well above the critical Al volume fraction  $\phi_c$ , where the films are metallic in behaviour, the morphology is often described as a continuous Al metallic matrix containing isolated inclusions of the amorphous insulating Ge. Below the metal–insulator transition (MIT), where the insulating films display variable-range hopping in their electronic transport properties, the structure is described as an insulating amorphous Ge matrix containing isolated Al metallic inclusions. Since at room temperature the resistivity does not display any discontinuity as the metal–insulator transition is crossed by varying the Al volume fraction, it is not obvious where the value for the critical metallic fraction  $\phi_c$  lies [1]. Some special techniques have been proposed for determining  $\phi_c$  in this case [2]. However, one must surmise that the changeover from isolated Al grains in a Ge matrix to isolated Ge grains in an Al matrix is continuous.

In the granular Al–Ge films, the Al grains exhibit superconductivity at enhanced temperatures of 1.6 K, both in the metallic films and also in the insulating films [3]. In the metallic films, the superconducting Al grains are connected by very thin metallic links. This

is because a relatively large 1.5 T magnetic field is required to quench the superconductivity which indicates the small-diameter grains and links. In the more insulating films, the superconductivity in the isolated Al grains produces a spectacular rise in the resistivity below  $T_c$  owing to the condensation of electrons into Cooper pairs, which limits the number of quasiparticles available for intergrain tunnelling. This phenomenon is known as Adkins hopping and leads to a large negative magnetoresistance [4]. For the insulating films located very close to the MIT, Josephson junction tunnelling currents electrically short out the intergrain (cluster) resistance as the temperature is decreased below  $T_c$  [3]. The current-carrying capacity of the Josephson junction network can be quenched by the application of a small 0.01 T field, resulting in a positive magnetoresistance. Thus owing to the unique behaviour of these two types of superconducting junction with applied magnetic field and temperature, one can experimentally separate out the metallic films from the insulating films and uniquely determine the critical Al concentration  $\phi_c$  in these granular films;  $\phi_c$  is typically 55 to 60 vol% Al.

The transport properties of the 'random' Al-Ge films are very different. Early pioneering work performed by Deutscher's group demonstrated that the 'random' structure is obtained by coevaporating Al and Ge onto heated glass substrates held at 180 °C rather than at room temperature [5, 6]. Since the Al and Ge grains possessed similar shapes and diameters of several hundred ångströms, the Al grains could not be distinguished topographically from the Ge grains in the electron microscope pictures, and this structure was described as 'random'. In a series of three important publications [1, 5, 6], this group showed that: (a) the random morphology was composed both of grains of Al and of crystalline grains of Ge in contrast to the amorphous Ge matrix in the granular structure; (b) the room temperature resistivity exhibited a sharp discontinuity at  $\phi_c$ ; and (c) the critical metallic volume fraction  $\phi_c$  for their morphology was close to the 15 vol% value predicted by continuum percolation theory for three-dimensional crystal and random lattices, composed of touching nearest-neighbour spheres [7]. However, neither the superconducting properties nor the normal-state transport properties at low temperatures of the random Al-Ge morphology were studied. The sharp discontinuity of the room temperature resistivity at the MIT enables the critical metallic volume fraction  $\phi_c$  to be easily identified from the experimental room temperature resistance data; this experimental value for  $\phi_c$  can now be compared with the results obtained from other techniques for predicting  $\phi_c$  [2].

## 2. Film fabrication and characterization

Thin 3500 Å granular Al-Ge films were fabricated on slices of microscope glass slides by coevaporating Al and Ge simultaneously using two electron guns [3]. Typical evaporation rates were 1.5 Å s<sup>-1</sup> and 8 Å s<sup>-1</sup> for the Al and Ge sources. The evaporations were made in vacua of 10<sup>-5</sup> mm Hg or better, and the glass slices were held at room temperature in order to obtain the granular structure.

The granular Al-Ge films were converted to the 'random' morphology by heating the films to 390 °C in a vacuum of 10<sup>-6</sup> mm Hg and allowing the films to slowly cool back to room temperature over a period of one day. Above 150 °C, the amorphous Ge diffuses away from the Al grains and crystallizes to form Ge clusters [8, 9, 10]. Since the thermal cycling sequence greatly influenced the critical Al fraction  $\phi_c$  at which the metal-insulator transition occurs, all of the films in each new series were cycled simultaneously together in a specially constructed stainless-steel vacuum cell sealed with a copper 'O' ring.

A similar procedure was followed for the samples studied in the transmission electron microscope (TEM). Thin 1000 Å granular Al-Ge films were deposited onto photoresist-coated slides; the thin films were lifted off the slide using acetone and floated onto fine nickel grids used for mechanically supporting the fragile films in the TEM. These grids were

transferred to the thermal-cycling cell where the films were heated to 390 °C in vacuum and converted to the 'random' structure.

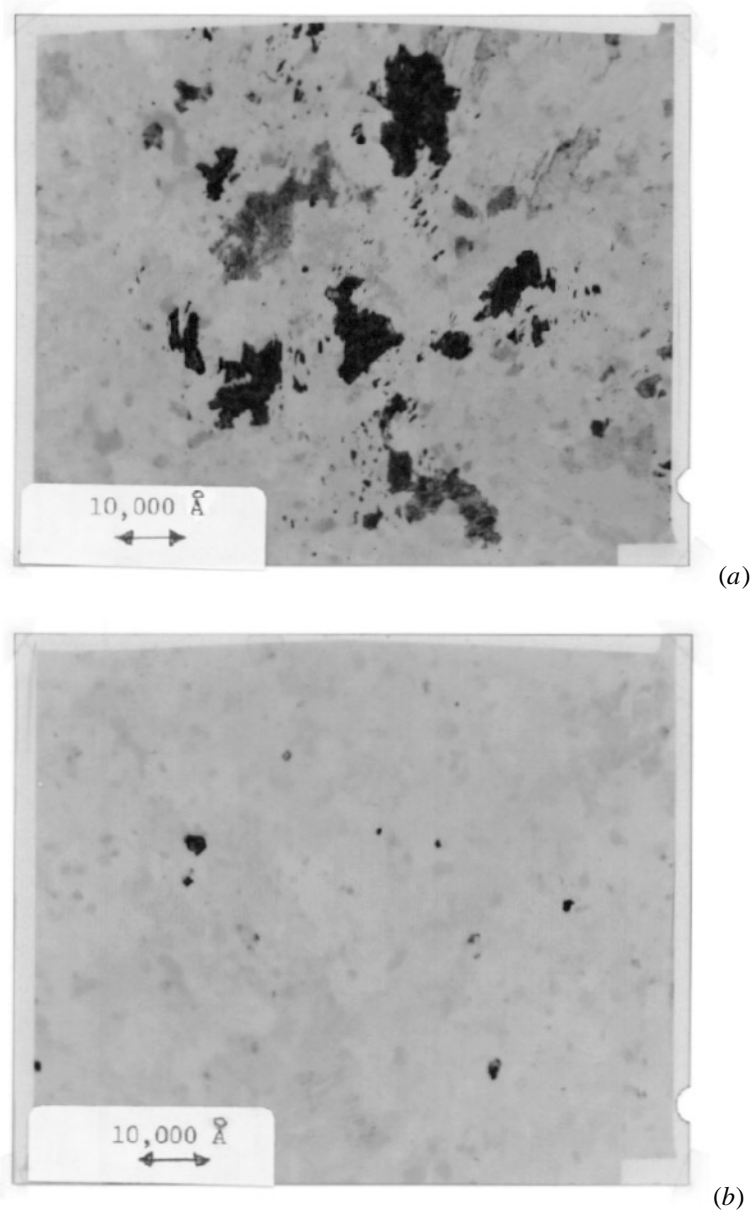


**Figure 1.** TEM micrographs taken for a 15 vol% Al film: (a) a dark-field image of the large Ge clusters; (b) a dark-field image of the small Al grains.

Dark-field micrographs from the TEM show that the typical dimensions of the crystalline Ge clusters are large and of the order of 15 000 Å to 20 000 Å for the film located just above the MIT having 9.2 vol% Al. The typical diameters of the Al grains are very small and of the order of 30 Å or less, as no structure is observed in the dark-field Al images, and the Al diffraction rings are not present. In contrast, for a more metallic film having 15 vol%

Al, the typical Ge cluster dimension is smaller, about 5000 Å, as seen in the dark-field micrograph of figure 1(a). The Al grains are much larger and of the order of 500 to 2000 Å as illustrated in figure 1(b). Al diffraction rings are observed.

Our thermal-cycling procedure differs from that in the earlier studies in which lower conversion temperatures of 180 °C were used, resulting in much smaller grains of Ge of 200 Å diameter [5, 6]. Because of this structure difference, our resistivity data and critical metallic fractions  $\phi_c$  differ from earlier published results [5, 6].

Energy-dispersive x-ray analysis (EDAX) of the Al and Ge contents was performed using a Link AN10000 EDS system attached to a JSM-840 SEM. The x-ray spectra were collected from five different regions along the length of each film, each region being of area 0.023 mm<sup>2</sup>. The analyses were carried out at 4.13 kV in order to contain most of the analysis volume within the film and to avoid the Si peaks. Correction was made for the typically 1% contribution from the substrate. The data were quantified using a bulk correction routine (ZAF-4/FLS) using pure element standards. We believe that the absolute concentrations are known, at worst, to an accuracy of  $\pm 10\%$ , for the case of films containing less than 10% Al. However, the relative concentrations between different films are known with much better accuracy, of  $\pm 2\%$ .

The Al fractions derived from the Link are given in units of atomic per cent, as the ratios of the number of Al atoms to the total number of atoms present in the film. As percolation and other theories refer to volume per cent rather than atomic per cent, the atomic fractions were converted to volume fractions  $\phi$  using the expression

$$\begin{aligned}\phi(\text{Al vol.}\%) &= 100/(1 + 1/y) \\ y &= \{\rho_{Ge}N_{Al}x/100\}/\{\rho_{Al}N_{Ge}(1 - x/100)\} = 0.73x/(100 - x)\end{aligned}\quad (1)$$

where  $x$  represents the amount of Al in atomic per cent,  $\rho$  is the density, and  $N$  is the atomic weight. The volume percentages are somewhat smaller than the atomic percentages. Typical atomic Al fractions ranged between 30 and 3 at.% and these values correspond to Al fractions of 24 to 2 vol%.

Indium tabs were pressed onto the films for electrical contacts. Measurements were made in a <sup>3</sup>He refrigerator and/or in a <sup>4</sup>He cryostat, both equipped with 4 T magnets.

### 3. Room temperature resistivity data

In figure 2, the room temperature resistivity is shown as a function of Al content in volume per cent. For the granular structure, all of the films are strongly insulating, since the critical volume fraction is above 50% Al. For the random structure, a spectacular jump in the resistivity, by a factor of 360, occurs between the two films having Al contents of 8.3 vol% and 9.2 vol% Al. Thus, the critical Al fraction at the metal-insulator transition (MIT) is somewhere between these two values, or at  $\phi_c = 8.8$  vol% Al if one takes the mean value. Different series will have different values for  $\phi_c$ , depending on the details of the thermal-cycling procedure. However, this material is unique in that the transition between metallic and insulating films is so abrupt that the critical fraction  $\phi_c$  can be uniquely identified for each series, using simple room temperature resistance measurements.

The present value for the critical metallic volume fraction  $\phi_c$  is much smaller than the 15% value based upon the random and lattice models having insulating and conducting spheres of equal diameters [7]. Values of  $\phi_c$  below 15% can be accounted for by a number of models. Kusy showed that, if the conducting grains are finer than the insulating grains and if the conducting component coats the nonconducting ones with a percolating network, then this model can lead to  $\phi_c$  being less than 5%, if the ratio of the diameters is 30 or larger [11]. Our morphology satisfies this criterion. McLachlan proposed a grain consolidation growth model, where during the regrowth process the conducting material is deposited in

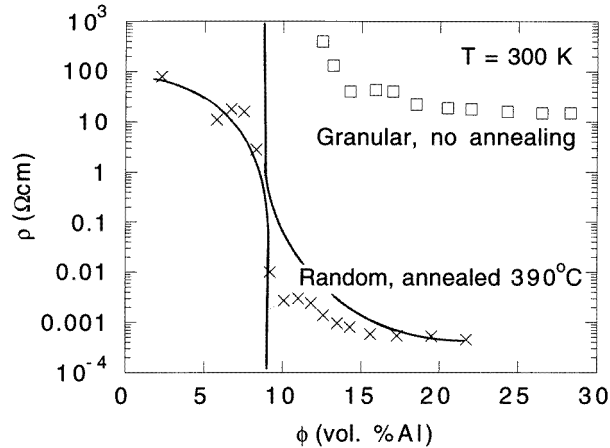


**Figure 2.** Resistivity at room temperature versus Al volume fraction for granular and random Al-Ge films. The granular films are all insulating. For the granular films, the MIT takes place above 50 vol% Al. Note the sharp discontinuity at 8.8 vol% Al in the random films where the metal-insulator transition takes place. The solid curves are predictions from the two percolation equations.

small blobs and fine links between the larger insulating grains [12]. This too gave a lower limit for  $\phi_c$  of less than 5%. Another way of achieving a low  $\phi_c$  is if the conducting particles are in the form of randomly oriented long rods or filaments [13]. An extreme case of this is in porous rocks where  $\phi_c$  is taken to be zero [14].

Imry *et al* have suggested that the critical metal fraction  $\phi_c$  in a percolating system should depend upon the finite film thickness  $t$  according to the power-law behaviour [15]

$$\phi_c(t) = \phi_c(3D) + (t_0/t)^{1/\nu} \quad (2)$$

where the 3D critical exponent  $\nu = 0.9$  [16, 17, 18] and  $t_0 = d$ , where  $d$  is the typical Al crystallite size. According to Kapitunik and Deutscher,  $t_0$  is  $170 + 90 \text{ \AA}$  (see [5, 6]), close to the values observed in the present samples just on the metallic side of  $\phi_c$ . If one uses  $t_0 = 170 \text{ \AA}$  and the measured film thickness of  $t = 3500 \text{ \AA}$ , then the corrected 3D value for  $\phi_c$  for a thick film drops to 5.3 vol% Al. This value is consistent with the lower theoretical limits for  $\phi_c$  [11, 12].

Percolation theory (see [19] and [20] and the references therein) predicts that the conductivity in the normal state should be given by  $\sigma(\phi) = \sigma_I[(\phi_c - \phi)/\phi_c]^{-s}$  below  $\phi_c$  and  $\sigma(\phi) = \sigma_C[(\phi - \phi_c)/(1 - \phi_c)]^t$  above  $\phi_c$ . Here  $\sigma_I$  and  $\sigma_C$  are the conductivities of the more insulating (Ge) and more conducting (Al) components respectively, and  $s$  and  $t$  are exponents. These equations hold only if  $\sigma_C \gg \sigma_I$  and are not valid in the interval near  $\phi_c$  of  $\Delta\phi = |\phi - \phi_c|^{1/(t+s)}$ . In this interval the general-effective-medium (GEM) equation, which reduces to the percolation equations in the limit where  $\sigma_I/\sigma_C \rightarrow 0$ , provided a successful fit over the entire composition range for the granular Al-Ge system [19, 20]. The GEM equation is

$$(1 - \phi)(\sigma_I^{1/s} - \sigma_M^{1/s})/(\sigma_I^{1/s} + A\sigma_M^{1/s}) + \phi(\sigma_C^{1/t} - \sigma_M^{1/t})/(\sigma_C^{1/t} + A\sigma_M^{1/t}) = 0$$

where  $\sigma_M$  is the conductivity of the composite material and  $A = (1 - \phi_c)/\phi_c$ .

The data for the random Al-Ge system were fitted both to the percolation equations and to the GEM equation. The parameters obtained were almost the same and well within the statistical errors. Figure 2 shows the fitted percolation equations with  $\phi_c =$

$0.0877 \pm 0.002$ ,  $t = 1.80 \pm 0.05$ ,  $s = 1.26 \pm 0.35$ ,  $\rho_C = 7.7 \mu\Omega \text{ cm}$  and  $\rho_I = 100 \pm 20 \Omega \text{ cm}$ . To get physically realistic values for all the parameters,  $\rho_C$  had to be fixed at the experimentally determined value of  $7.7 \mu\Omega \text{ cm}$ , known from measurements on thin pure Al films. The value of  $\phi_c$  and the one obtained from the GEM equation are almost identical to the arithmetic mean value of 0.088. The value for  $t$  is close to the universal value of 1.9 predicted from 3D percolation theory [21] but is considerably greater than the value of 1.3 derived from the 2D percolation theory [22]. Further details of these fits and discussions of the parameters are given in [23] and [24].

#### 4. Low-temperature conductivity data for the metallic films

A common procedure for determining the critical metallic fraction  $\phi_c$  is to measure low-temperature conductivity data for the metallic films. Note that it is important to use ‘normal-state’ conductivity data, where all superconductivity phenomena have been suppressed by a sufficiently large magnetic field. Values for the zero-temperature conductivity  $\sigma(0)$  can then be obtained by extrapolating the data. Then from a plot of  $\sigma(0)$  versus  $\phi$ , the critical Al fraction  $\phi_c$  can be estimated by observing where  $\sigma(0)$  vanishes.

We assume that at sufficiently low temperatures, the conductivity can be described by the general expression

$$\sigma(T) = \sigma(0) + CT^x \quad (3)$$

where  $C$  is a prefactor and  $x$  is the exponent of the temperature power law. Equation (3) approximates the conductivity contributions from the 3D weak-localization theory [25, 26] and the 3D electron–electron interaction theory [27, 28]. Note that in our procedure  $x$  is a free fitting parameter and is not set to the value of 1/2 as predicted in the 3D electron–electron interaction theory [27, 28].

There are two procedures for determining the exponent  $x$  [2]. If three values of the conductivity are known at temperatures  $T_1$ ,  $T_2$ , and  $T_3$ , then the following equality must be satisfied:

$$[\sigma(T_1) - \sigma(T_2)]/[\sigma(T_2) - \sigma(T_3)] = [T_1^x - T_2^x]/[T_2^x - T_3^x]. \quad (4)$$

By guessing an appropriate value for  $x$ , the equality can be satisfied, and afterwards the other two parameters,  $C$  and  $\sigma(0)$ , can easily be found.

Our second new procedure for determining the exponent  $x$  is similar to that suggested by Hill and by Zabrodskii and Zinov’eva for insulating films [29, 30]. We begin by calculating values of  $\omega(T)$  from the resistivity data on the metallic films in the normal state, where

$$\omega(T) = -d \ln \rho / d \ln T. \quad (5)$$

When substituting equation (3) into equation (5) and using  $\rho(T) = 1/\sigma(T)$ , we find that

$$\omega(T) = xCT^x/\sigma(T) = \rho(T)xCT^x. \quad (6)$$

By taking logarithms on both sides of equation (6), and transposing, we obtain

$$\ln \omega(T) - \ln \rho(T) = \ln(xC) + x \ln T. \quad (7)$$

Equation (7) is that of a straight line of the form  $z = I_0 + Sy$ ; in fitting a linear regression fit through the  $\ln \omega - \ln \rho$  versus  $\ln T$  data, the slope  $S$  is equal to the exponent  $x$  and the intercept  $I_0$  is related to the prefactor  $C$  through the expression  $C = (\exp I_0)/x$ . This procedure predicts values for  $x$  within 10% of those obtained from the above interpolation method using equation (4). Note that both methods predict unbiased values for the exponent  $x$ ; and hence both methods yield the most accurate, but model-independent, values for the zero-temperature conductivity  $\sigma(0)$ . It should also be noted that both methods work only on

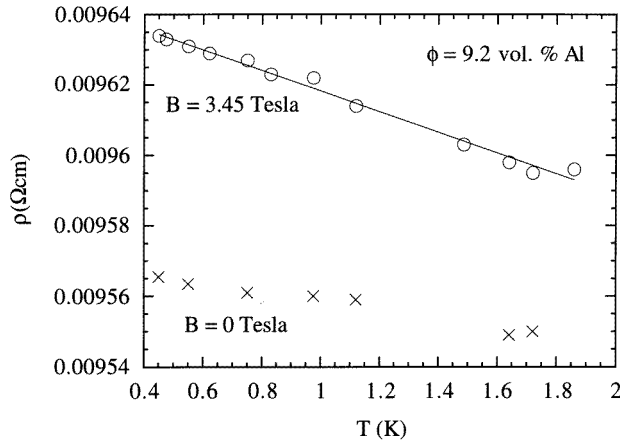


**Figure 3.** Resistivity versus temperature for the first metallic film located just above the metal-insulator transition (9.2 vol% Al). Observe that the zero-field data display no signatures of superconductivity. The solid line through the 3.45 T data is a power-law fit according to  $\sigma = 1/\rho = 103.7 + 0.270T^{1.20}$  in units of  $\Omega^{-1} \text{ cm}^{-1}$ .

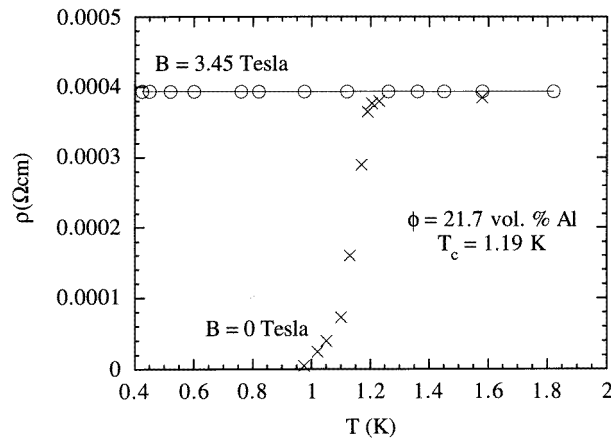


**Figure 4.** Resistivity versus temperature for a very metallic film (21.7 vol% Al). Observe the 'rounding' of the zero-field resistivity above 1.2 K due to superconducting fluctuations in the Al grains and notice the small 'resistive tail' below 1.2 K arising from Josephson junction links between the Al grains. The solid line through the normal-state data is a power-law fit according to  $\sigma = 1/\rho = 2540 + 1.32T^{0.97}$  in units of  $\Omega^{-1} \text{ cm}^{-1}$ .

resistivity data that increase with decreasing temperature. Figure 3 shows a fit obtained using equation (3) to a metallic film very close to the MIT (9.2% Al) and figure 4 demonstrates a fit to a very metallic film (21.7% Al); the two straight lines appearing in figures 3 and 4 are  $\rho(\Omega \text{ cm}) = (103.7 + 0.270T^{1.20})^{-1}$  and  $\rho(\Omega \text{ cm}) = (2540 + 1.32T^{0.97})^{-1}$ . Experimental values for the exponent  $x$  are shown in figure 5 and are twice as large as the accepted theoretical prediction [27, 28]. Values of the zero-temperature conductivity  $\sigma(0)$  versus  $\phi$  from the various metallic films are plotted in figure 6. The critical Al volume fraction  $\phi_c$  where  $\sigma(0)$  vanishes is approximately  $9.0 \pm 0.4$  vol% Al, consistent with the 8.8 vol% value obtained from the room temperature resistivity data. Thus, the low-temperature resistivity

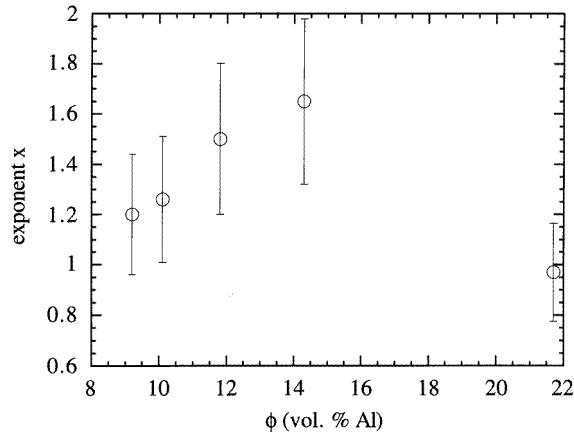


**Figure 5.** The exponent  $x$  of the temperature power-law term as a function of Al content; the measured values are considerably greater than the value of  $1/2$  predicted from the electron–electron interaction theory.

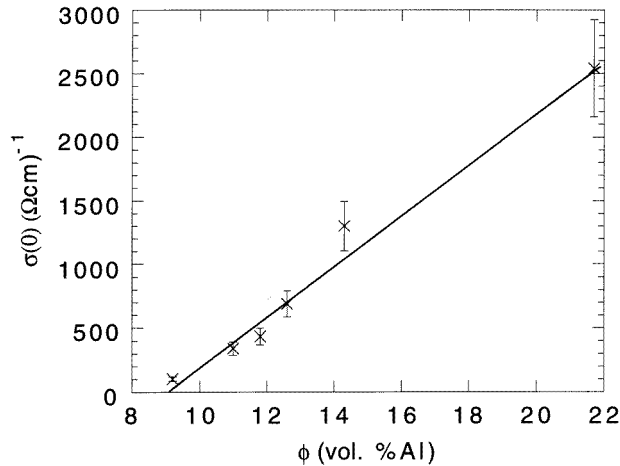


**Figure 6.** The zero-temperature conductivity  $\sigma(0)$  as a function of Al content. Values for  $\sigma(0)$  were obtained using a new fitting technique described in the text. The Al fraction  $\phi$ , where the conductivity vanishes, defines the critical volume fraction  $\phi_c$  at the metal–insulator transition. In this case,  $\phi_c = 9.0 \pm 0.4$  vol% Al. The solid line is a linear regression fit through the data.

data can provide another good estimation of  $\phi_c$ . The  $\sigma(0)$  data can be fitted to the expression  $\sigma(0) = \sigma_0(\phi - \phi_c)^t$  where  $\sigma_0 = 189 \Omega^{-1} \text{cm}^{-1}$  and  $t = 1.02$ , somewhat smaller than the 2D percolation value of  $t = 1.3$  [22].

## 5. Properties of the insulating films

The insulating films below the MIT exhibited such strong activated hopping in the resistivity that the resistivity measurements were restricted to between 100 K to 425 K. As shown in figure 7, the resistivity of the 2.3 vol% Al film follows a Mott variable-range-hopping law

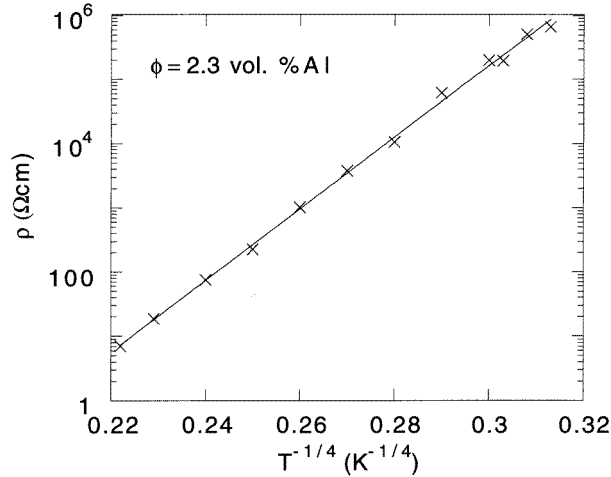


**Figure 7.** Resistivity versus temperature for the most insulating film (2.3 vol% Al). The solid line represents a Mott variable-range-hopping fit to the data.

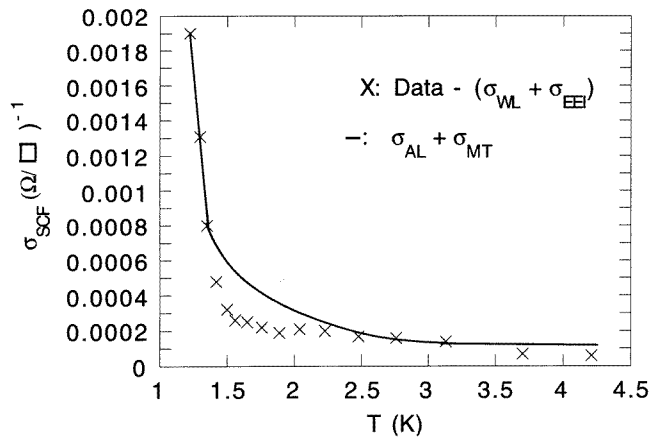


**Figure 8.** Superconducting fluctuation conductivity versus temperature in zero field for a 21.2 vol% Al film. The solid line includes contributions from the zero-field 2D Aslamazov–Larkin and Maki–Thompson theories with the single fitting parameter,  $T_c$  chosen to be 1.19 K, the superconducting transition temperature for bulk Al.

$\rho(T) = \rho_0 \exp(T_{Mott}/T)^{1/4}$  with  $T_{Mott} = 2.6 \times 10^8$  K and  $\rho_0 = 3.51 \times 10^{-12}$   $\Omega$  cm. The transition region was so sharp that it was not possible to obtain values for the effective temperature  $T_{eff}$  as a function of  $\phi$  just below the MIT; thus, it was not possible to extrapolate  $T_{eff}$  to zero in order to obtain an additional estimation for the critical volume fraction  $\phi_c$  from the insulating side, as was done for granular Al–Ge [3]. It is interesting to note that for the more insulating random Al–Ge films, one obtains the Mott exponent of 1/4; in contrast, for the more insulating granular Al–Ge films, the hopping exponent is the Efros–Shklovskii value of 1/2. Why the microstructure of the granular material involves Coulomb interactions and that of the random material does not remains an open question. Additional experimental work is needed to characterize the insulating films.

## 6. Superconducting fluctuation measurements

Superconducting fluctuations are responsible for the ‘rounding’ of the resistance curves above the superconducting temperature  $T_c$ . The transition temperature  $T_c$  generally refers to the bulk transition of the entire film. The superconducting fluctuation (SCF) conductivity  $\sigma_{SCF}$ , also known as paraconductivity or excess conductivity, can often be observed at temperatures as high as  $4T_c$ . Above 4.2 K, the superconducting fluctuation conductivity is negligible in our ‘random’ Al–Ge films, when compared to the antilocalization conductivity  $\sigma_{WL}$  arising from spin–orbit scattering and to the electron–electron interaction conductivity,  $\sigma_{EEI}$ . In order to obtain accurate values for the zero-field SCF conductivity, it is important to extend the zero-field measurements up to 20 K and then to extrapolate the data taken between 5 K and 20 K down to 1 K. The difference between the zero-field data taken below 4.2 K and this extrapolated ‘normal-state’ conductivity line represents the SCF conductivity contribution. Alternatively, we have quenched the superconducting fluctuations by applying a small 1 T field and then calculated values for  $\sigma_{SCF}$  by taking differences between data measured in zero field and data measured in the field. Typical zero-field SCF data for a 14.3% random Al–Ge film having  $R_{\square} = 12 \Omega/\square$  are shown in figure 8. The magnitudes for  $\sigma_{SCF}$  are small above 2 K but increase significantly at around 1.2 K. Details on the theoretical SCF expressions can be found in [31]. Using the 2D Aslamazov–Larkin and the 2D Maki–Thompson conductivity expressions, a reasonably good fit to the data (the solid line in figure 8) can be obtained only if the single fitting parameter  $T_c$  is chosen equal to 1.19 K; this temperature coincides with the transition temperature of bulk Al. The reason that the 2D SCF theories were selected is that the Ginzburg–Landau superconducting coherence length  $\xi_{GL}(T)$  is considerably greater than the typical Al grain and cluster dimension and is somewhat greater than the film thickness. Values for the pair-breaking parameter  $\delta(T)$  that appears in the Maki–Thompson expression were calculated from the scattering time expressions that appear in [31].

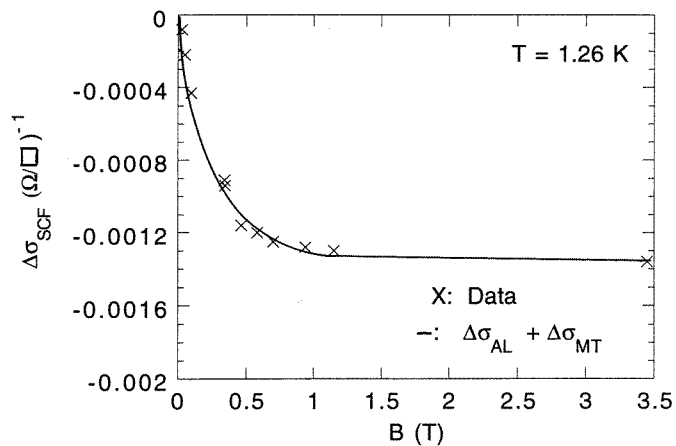


**Figure 9.** Magnetoconductance data versus magnetic field taken slightly above  $T_c = 1.19$  K. The theories of Redi for the 2D Aslamazov–Larkin contribution and of Lopes dos Santos and Abrahams for the 2D Maki–Thompson contribution were used. The only fitting parameter was  $T_c$ , chosen to be 1.19 K.

The magnetoconductance data  $\Delta\sigma_{SCF}$  could be fitted nicely incorporating the important Maki–Thompson MC expression of Lopes dos Santos and Abrahams and the Aslamazov–

Larkin MC expression of Redi (see [32, 33]). Refer to [31] for the appropriate expressions. The fitting results are shown in figure 9 where the only fitting parameter was  $T_c$ , fixed at 1.19 K. The diffusion constant  $D$  was required to evaluate the Lopes dos Santos–Abrahams expression and was known to be  $1.8 \text{ cm}^2 \text{ s}^{-1}$  from critical field measurements made below 1.19 K in very metallic films [31].

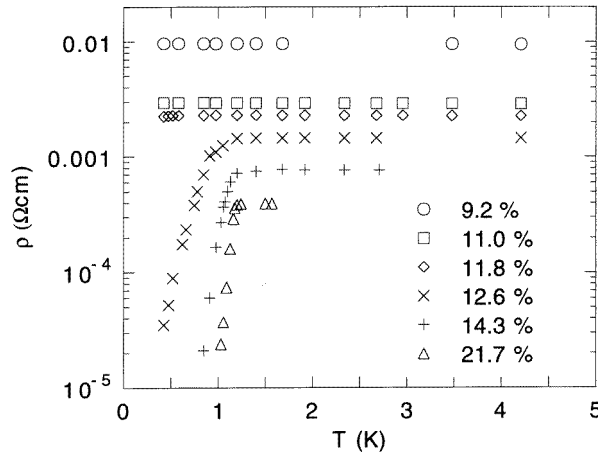


**Figure 10.** A summary of the low-temperature, zero-field, resistivity data for metallic films located above the metal–insulator transition. Notice the transition from the superconducting state to the normal-metallic state at 0.5 K as the Al content is reduced. The ‘resistive tails’ are clearly seen in the more metallic films below 1.2 K.

According to the SCF theories, metallic regions that display SCFs well above  $T_c$  should make transitions to zero resistivity at  $T_c$ . Had both the Al grains and the links between the grains exhibited SCFs, the films would have had a zero resistivity at  $T_c = 1.19 \text{ K}$ . Yet, inspection of the zero-field resistivity curves at  $T = 1.19 \text{ K}$  in figure 10 reveals that the resistivity of most of the films has decreased only by 10% or less from the normal-state resistivity. This behaviour suggests that only the Al grains make the superconducting transition at 1.19 K and that the links which connect the grains remain normal at 1.19 K. The observation of the ‘resistive tails’ below 1.19 K in figure 10 suggests the presence of two different types of link between the large Al clusters or blobs: (a) thick discontinuous links that form Josephson tunnelling junctions; and (b) thin continuous normal-metallic links which never go superconducting. As the temperature is decreased below 1.19 K, more and more of the Josephson tunnelling junctions will go superconducting as the characteristic energy  $E_J$  of each junction exceeds  $k_B T$ . These junctions will short out the normal links that are in parallel with them, thus giving rise to the ‘resistive tail’ behaviour.

## 7. The phase diagram for random Al-Ge films

Figure 10 shows the zero-field resistivity data as a function of temperature for six samples between 9.2 and 21.7 vol% Al. In the cases where the Josephson tunnelling junctions couple the Al clusters, the resistivity will decrease below  $T_c$ . In the very metallic films having  $\phi > 35 \text{ vol}\% \text{ Al}$ , superconducting fluctuations are present above 1.19 K, producing a pronounced ‘rounding’ of the resistance curves, followed by sharp superconducting transitions to zero resistivity at 1.19 K, the bulk transition temperature for Al (not shown in figure 10). Both the Al grains and the links participate in this sharp transition. As the Al

content is decreased below 25 vol% Al, the superconducting fluctuations are still present in the Al grains above 1.19 K while ‘resistive tails’ or rapid broadening of the resistance transition curves occurs below 1.19 K, owing to the presence of the Josephson tunnelling junctions in parallel with normal-metallic links. The two films located just above the MIT (9.2% and 11.0%) exhibit only normal-metallic-state transport properties, characterized by weak 1% rises in the resistivity per temperature decade. The increase in the resistivity arises primarily from electron–electron interaction effects and antilocalization effects in the nonsuperconducting links. Either the clusters do not go superconducting or the transition is masked by the high resistances of the links.

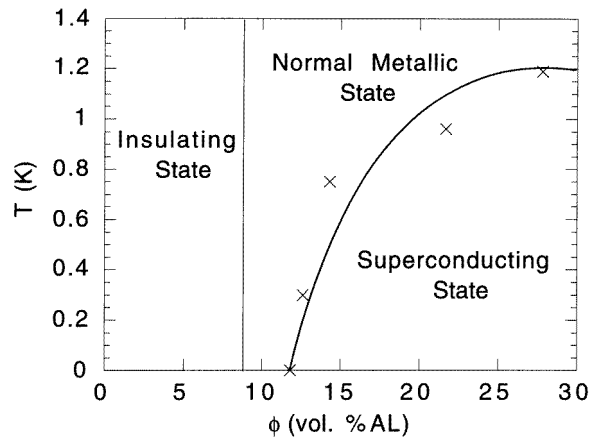


**Figure 11.** The schematic phase diagram for random Al–Ge films. Values for critical metallic fractions and superconducting transition temperatures will vary somewhat from series to series depending upon the thermal-cycling procedure.

The zero-field resistivity data of figure 10 are summarized in the phase diagram shown in figure 11. Deutscher has suggested that a transition from the superconducting state to the normal state occurs when the 3D percolation length  $\xi_{3D} = t_0/(\phi - \phi_c)^\nu$  exceeds the film thickness  $t$ , producing a transition from 3D to 2D as the Al content  $\phi$  is reduced to  $\phi_c$ . The fluctuations in the superconducting order parameter are considerably greater in 2D than in 3D. Thus, superconductivity can be quenched if the film is in the 2D region. This normal-state region should then extend over the Al content width  $(\phi - \phi_c) = (t_0/t)^{1/\nu}$ . For films with  $t = 3500 \text{ \AA}$  consisting of  $170 \text{ \AA}$  ( $t_0$ ) grains, the width is approximately 3 vol% Al, in agreement with the 3 vol% width observed in figure 11. Similar behaviours have been observed in amorphous niobium–silicon films [42], amorphous molybdenum–germanium films [43], and amorphous gold–silicon films [44].

Kusy has predicted that the resistivity of the first metallic film located just above the MIT should have its resistivity enhanced by a factor of  $100\%/\phi_c$  over the resistivity of the very metallic films [11]. Inspection of figures 2 and 10 reveals that the enhancement is of the order of 23, in nice agreement with Kusy’s prediction of 25.

We observe that the superconducting transition temperature in the random Al–Ge films is not enhanced over the 1.19 K transition temperature for bulk Al as it is in the granular Al–Ge films [3]. As both systems near  $\phi_c$  are made up of clusters consisting of small Al grains, one concludes that the amorphous Ge coatings around the Al grains in the granular morphology are partially responsible for the enhancement of  $T_c$ .

## 8. The ‘resistive tails’ below $T_c$

The more metallic films have ‘resistive tails’ below  $T_c = 1.19 \text{ K}$ , or exhibit broad transitions to zero resistivity as can be seen in figure 10. Note the shape of the tails—they are

hyperbolic or convex-lens-like in shape. The common theoretical explanation for the tail is the Kosterlitz–Thouless transition at  $T_{KT}$ , where the spontaneously generated current vortices coalesce to form bound pairs. The existence of a KT transition gives rise to a temperature-dependent resistance that follows the relation [34]

$$R/R_N = A \exp(-2(b\tau_{mf}/\tau)^{1/2}) \quad (8)$$

where  $\tau_{mf} = (T_{mf} - T_{KF})/T_{KF}$ ,  $t = (T - T_{KF})/T_{KF}$  and  $T_{mf}$  is the mean-field transition temperature of  $T_c = 1.19$  K. The Kosterlitz–Thouless transition temperature  $T_{KF}$  is treated as a fitting parameter. The mathematical reason for which equation (8) successfully fits many of the ‘tail’ data is the square-root dependence that appears in the exponent [35]. However, for this model to apply, the metallic grains must be large enough to support vortices. The size of the vortex core is typically the superconducting coherence length, which for Al is of the order of 16 000 Å—much larger than the typical Al grain dimension in our films. Thus, this model does not apply to individual small grains but may apply to large granular clusters. Also it is not obvious how one can introduce a magnetic field dependence into equation (8) to explain the dependence of the MC data taken below 1.19 K upon the applied field.

We propose an alternative model to explain the resistive tails, first proposed by Deutscher *et al* [36]. Some of the metallic links connecting the grains are continuous but too thin to support superconductivity. Other links between the same grains contain sufficient Al to form superconducting Josephson tunnelling junctions and weak links. When the thermal energy  $E_T = k_B T$  is reduced below the Josephson coupling energy,  $E_J(T)$  [37],

$$E_J(T) = (\pi\hbar/4e^2 R_N) \Delta_{BCS}(T) \tanh[\Delta_{BCS}(T)/2k_B T] \quad (9)$$

by cooling the junction sufficiently below  $T_c$ , the junction will short out the parallel normal-metallic link and connect the two superconducting Al grains with a zero-resistivity path. In equation (9),  $\Delta_{BCS}(T)$  is the temperature-dependent BCS energy gap, tabulated by Muhlschlegel [38], and  $R_N$  is the normal-state resistance of the junction, taken as a fitting parameter. For example, a Josephson junction having a normal-state resistance of  $R_N = 4900 \Omega$  will have a transition temperature of  $T = 0.85$  K. The percolation problem of coupled Josephson junctions has been partially solved by Simanek who predicts in figure 2 of [39] the resistance dependence of Josephson connected bonds upon temperature. The difficulty with his prediction is that the temperature dependence of the resistivity takes on the form of a parabolic or concave-lens-like shape, which is not observed experimentally. However, Simanek did not consider normal-state bonds in parallel with the Josephson connected bonds [39]. If one includes these ‘two parallel resistors’ in the model, computer modelling suggests that the resistance versus temperature curve will take on a hyperbolic or convex-lens-like shape, in agreement with the experimental data. We are not qualified to produce a rigorous theory. Moreover, one should try to incorporate the BCS energy gap into the theory, since there are several predictions for the depression of the BCS energy gap with applied magnetic field, which would allow one to also predict the dependence of the negative magnetoconductance data upon applied magnetic field observed below  $T = 1.19$  K [40, 41]. More theoretical work is needed on this problem.

### Acknowledgments

We are very grateful to Drs E Buchstab, M Slutzky and Y Ashkenazy for participation in the initial measurements. We greatly benefited from discussions with Professor G Deutscher, Professor Y Kantor, and Dr M Rappaport. We are obliged to the German–Israeli Foundation (GIF) and to the Internal Research Fund of Tel Aviv University for financial support.

We thank Mrs Rachel Rosenbaum for editing assistance. We acknowledge the computing facilities of the University of Cambridge Computing Service.

## References

- [1] Deutscher G, Rappaport M and Ovadyahu Z 1978 *Solid State Commun.* **28** 593
- [2] Rosenbaum R, Slutzky M, Mobius A and McLachlan D S 1994 *J. Phys.: Condens. Matter* **6** 7977
- [3] Eytan G, Rosenbaum R, McLachlan D S and Albers A 1993 *Phys. Rev. B* **48** 6342
- [4] Adkins C J, Thomas J M D and Young M W 1980 *J. Phys. C: Solid State Phys.* **13** 3427
- [5] Kapitulnik A, Rappaport M L and Deutscher G 1981 *J. Physique Lett.* **42** L541
- [6] Kapitulnik A and Deutscher G 1983 *J. Phys. A: Math. Gen.* **16** L255
- [7] Scher H and Zallen R 1970 *J. Chem. Phys.* **53** 3759
- [8] Li Bo-quan, Zheng Bin, Zhang Shu-yuan and Wu Zi-qin 1993 *Phys. Rev. B* **47** 3638
- [9] Deutscher G and Lereah Y 1988 *Phys. Rev. Lett.* **60** 1510
- [10] Lereah Y, Deutscher G and Grunbaum E 1991 *Phys. Rev. A* **44** 8316
- [11] Kusy R P 1977 *J. Appl. Phys.* **48** 5301
- [12] McLachlan D S 1991 *J. Appl. Phys.* **70** 3681
- [13] Carmona F, Prudhon P and Barreau F 1984 *Solid State Commun.* **51** 255
- [14] Bergman D and Stroud D 1992 *Solid State Physics* vol 46, ed H Ehrenreich and D Turnbull (San Diego, CA: Academic) pp 171, 231
- [15] Imry Y, Deutscher G, Bergman D J and Alexander S 1973 *Phys. Rev. A* **7** 744
- [16] Kirkpatrick S 1973 *Rev. Mod. Phys.* **45** 574
- [17] Hoshen J, Kopelman R and Mongerg E M 1978 *J. Stat. Phys.* **19** 219
- [18] Heermann D W and Stauffer D 1981 *Z. Phys. B* **44** 339
- [19] McLachlan D S, Rosenbaum R, Albers A, Eytan G, Grammatica N, Hurvits G, Pickup J and Zaken E 1993 *J. Phys.: Condens. Matter* **5** 4829
- [20] McLachlan D S, Blaszkiewicz M and Newnham R E 1990 *J. Am. Ceram. Soc.* **73** 2187
- [21] Derrida B, Stauffer D, Herrmann H J and Vannimenes J 1983 *J. Physique. Lett.* **44** L701
- [22] Herrmann H J, Derrida B and Vannimenes J 1984 *Phys. Rev. B* **30** 4080
- [23] McLachlan D S 1996 *Electrically-based Microstructural Characterization; MRS Proceedings* vol 411, ed R A Gerhardt, S R Taylor and E J Garboczi (Pittsburgh, PA: Materials Research Society) at press
- [24] McLachlan D S and Rosenbaum R 1996 *Electrically-based Microstructural Characterization; MRS Proceedings* vol 411, ed R A Gerhardt, S R Taylor and E J Garboczi (Pittsburgh, PA: Materials Research Society) at press
- [25] Fukuyama H and Hoshino K 1981 *J. Phys. Soc. Japan.* **50** 2131
- [26] Baxter D V, Richter R, Trudeau M L, Cochrane R W and Strom-Olsen J O 1989 *J. Physique* **50** 1673
- [27] Altshuler B L and Aronov A G 1983 *Solid State Commun.* **46** 429
- [28] Lee P A and Ramakrishnan T V 1985 *Rev. Mod. Phys.* **57** 308
- [29] Hill R M 1976 *Phys. Status Solidi a* **35** K29
- [30] Zabrodskii A G and Zinov'eva K N 1984 *Zh. Eksp. Teor. Fiz.* **86** 727 (Engl. Transl. 1984 *Sov. Phys.-JETP* **59** 425)
- [31] Zaken E and Rosenbaum R 1994 *J. Phys.: Condens. Matter* **6** 9981
- [32] Lopes dos Santos J M B and Abrahams E 1985 *Phys. Rev. B* **31** 172
- [33] Redi M H 1977 *Phys. Rev. B* **16** 2027
- [34] Mooij J E 1983 *Percolation, Localization, and Superconductivity* ed A M Goldman and S A Wolf (New York: Plenum) p 325
- [35] Vadlamannati S, Li Q, Venkatesan T, McLean W L and Lindenfeld P 1991 *Phys. Rev. B* **44** 7094
- [36] Deutscher G, Entin-Wohlman O, Fishman S and Shapira Y 1980 *Phys. Rev. B* **21** 5041
- [37] Ambegaokar V and Baratoff A 1963 *Phys. Rev. Lett.* **10** 486 (1963 errata **11** 104)
- [38] Muhlschlegel B 1959 *Z. Phys.* **155** 313
- [39] Simanek E 1982 *Phys. Rev. B* **25** 237
- [40] Mathur V S, Panchapakesan N and Saxena R P 1962 *Phys. Rev. Lett.* **9** 374
- [41] Douglass D H Jr 1961 *Phys. Rev. Lett.* **6** 346
- [42] Hertel G, Bishop D J, Spencer E G, Rowell J M and Dynes R C 1983 *Phys. Rev. Lett.* **50** 743
- [43] Yoshizumi S, Mael D, Geballe T H and Greene R L 1985 *Localization and Metal-Insulator Transitions* ed H Fritsche and D Adler (New York: Plenum) p 77
- [44] Furubayashi T, Nishida N, Yamaguchi M, Morigaki K and Ishimoto H 1985 *Solid State Commun.* **55** 513